

## Revealing the Milky Way’s Thick Disk and Halo Ultracool Dwarf Populations with Roman

AARON M. MEISNER,<sup>1</sup> RUSSELL E. RYAN,<sup>2</sup> S. K. LEGGETT,<sup>3</sup> JOSHUA E. SCHLIEDER,<sup>4</sup> CHRISTOPHER A. THEISSEN,<sup>5</sup>  
ADAM J. BURGASSER,<sup>6</sup> DAN CASELDEN,<sup>7</sup> ADAM C. SCHNEIDER,<sup>8</sup> EDUARDO L. MARTÍN,<sup>9</sup> I. NEILL REID,<sup>2</sup>  
CHRISTIAN AGANZE,<sup>5</sup> JOHN E. GIZIS,<sup>10</sup> EILEEN C. GONZALES,<sup>11,\*</sup> SARAH E. LOGSDON,<sup>1</sup> FEDERICO MAROCCO,<sup>12</sup>  
WEI-CHUN JAO,<sup>13</sup> JOAN R. NAJITA,<sup>1</sup> AND ARJUN DEY<sup>1</sup>

<sup>1</sup>NSF’s National Optical-Infrared Astronomy Research Laboratory, 950 N. Cherry Avenue, Tucson, AZ 85719, USA

<sup>2</sup>Space Telescope Science Institute, 3700 San Martin Drive, Baltimore, MD 21218, USA

<sup>3</sup>Gemini Observatory/NSF’s NOIRLab, 670 N. A’ohoku Place, Hilo, HI 96720, USA

<sup>4</sup>NASA Goddard Space Flight Center, Greenbelt, MD 20771, USA

<sup>5</sup>Center for Astrophysics and Space Sciences, UC San Diego, 9500 Gilman Drive, La Jolla, CA 92093-0424, USA

<sup>6</sup>Department of Astronomy & Astrophysics, UC San Diego, 9500 Gilman Drive, La Jolla, CA 92093, USA

<sup>7</sup>Department of Astrophysics, AMNH, Central Park West at 79th Street, New York, NY 10024, USA

<sup>8</sup>United States Naval Observatory, Flagstaff Station, 10391 West Naval Observatory Rd., Flagstaff, AZ 86005, USA

<sup>9</sup>Instituto de Astrofísica de Canarias, Calle Vía Láctea s/n, E-38200 La Laguna, Tenerife, Spain

<sup>10</sup>Department of Physics and Astronomy, University of Delaware, Newark, DE 19716, USA

<sup>11</sup>Department of Astronomy and Carl Sagan Institute, Cornell University, 122 Sciences Drive, Ithaca, NY 14853, USA

<sup>12</sup>IPAC, Mail Code 100-22, Caltech, 1200 E. California Blvd., Pasadena, CA 91125, USA

<sup>13</sup>Department of Physics and Astronomy, Georgia State University, Atlanta, GA 30303, USA

### 1. COVER PAGE INFORMATION

**Roman Core Community Survey:** High Latitude Wide Area Survey

**Scientific Category:** stellar physics and stellar types

**Submitting Author:** Aaron Meisner, NSF’s NOIRLab, [aaron.meisner@noirlab.edu](mailto:aaron.meisner@noirlab.edu)

**Scientific Keywords:** Brown dwarfs, M dwarfs, L dwarfs, T dwarfs, Metallicity, Milky Way stellar halo

### 2. SCIENTIFIC MOTIVATION/OVERVIEW

In the solar neighborhood and in young clusters, the mass function shows a continuum from dwarf stars with masses of tenths of a solar mass ( $M_{\odot}$ ) to brown dwarfs (objects with insufficient mass for hydrogen burning) with masses of a few Jupiter masses ( $M_J$ ; e.g., Gagné et al. 2017; Kirkpatrick et al. 2019, 2021; Lodieu et al. 2021; Luhman & Hapich 2020). Distant  $\sim 0.1M_{\odot}$  objects have been found via microlensing in the Galactic bulge (Chung et al. 2017) and in deep HST/JWST imaging and spectroscopy (Ryan et al. 2005; Aganze et al. 2022). Analysis of Gaia (Lindgren et al. 2008) transverse velocities and Hertzsprung–Russell diagrams shows that a very low mass (VLM) population with masses down to  $0.2M_{\odot}$  exists in all components of the Galaxy (Hallakoun & Maoz 2021). Furthermore, in the VLM star regime, the favored initial mass function increases toward lower masses (e.g., Chabrier 2003; Kroupa 2001).

VLM stars and brown dwarfs are intrinsically faint, due to their small sizes and low effective temperatures ( $T_{\text{eff}}$ ), hence most studies of brown dwarfs have thus far been limited to the solar neighborhood. Such studies show that brown dwarfs with  $T_{\text{eff}} \lesssim 1000$  K typically range in mass from 5 to 50  $M_J$  (though recent findings suggest mid-late T dwarfs can be heavier than 50  $M_J$  e.g., Brandt et al. 2020), in metallicity ( $[m/H]$ ) from  $-0.5$  to  $+0.3$  dex, and in age from 0.5 to 5 Gyr (Leggett et al. 2021; Line et al. 2017). Not surprisingly, the metallicity and age range of the sample is typical of the thin disk (Kilic et al. 2019; Hallakoun & Maoz 2021). Despite their pervasiveness, many questions remain regarding the properties of the lowest luminosity objects in our Milky Way Galaxy. For example, (1) how has the birth rate of VLM stars and brown dwarfs evolved over time, from early periods of star formation to the present epoch, and (2) how do brown dwarf atmospheres and spectral energy distributions (SEDs) change with temperature, metallicity, and age? Identifying and characterizing metal-poor ultracool dwarfs is key to answering these questions.

\* 51 Pegasi b Fellow

Nancy Grace Roman Space Telescope (Roman) Wide Field Instrument (WFI) imaging across a wide area (thousands of square degrees) has the potential to dramatically expand the volume over which we can detect/select ultracool dwarfs, particularly into the substellar regime, with sample selection being a primary challenge. As described in §3, it is important for this science application that the Roman High Latitude Wide Area Survey (HLWAS) include imaging in Roman WFI’s  $K$ -band equivalent filter (F213), as this bandpass is critical for photometric selection of distant, metal-poor ultracool dwarfs in the Milky Way’s thick disk and halo. Euclid’s Wide Survey (Euclid Collaboration et al. 2022) will not cover the sky in a photometric band redder than their  $H$  filter ( $1.5 < \lambda/\mu\text{m} < 2.0$ ), so this is an especially critical and unique science opportunity for Roman.

### 3. OPTIMIZING ROMAN’S HIGH LATITUDE WIDE AREA SURVEY FOR DISTANT ULTRACOOL DWARFS

The  $K$ -band wavelength region  $\approx 2.03\text{--}2.38 \mu\text{m}$  is crucial for the photometric selection of low-metallicity ultracool dwarfs in the Milky Way’s thick disk and halo. Collision induced absorption (CIA) from  $\text{H}_2$ , which is intrinsically pressure- and metallicity-sensitive, is more pronounced in low-metallicity ultracool dwarf atmospheres than in solar metallicity equivalents (e.g., Linsky 1969; Borysow et al. 1997; Burgasser et al. 2002), resulting in a signature suppression of  $K$ -band flux (see Figure 1). Broadband photometric techniques for selecting distant, low-metallicity ultracool dwarfs into the Milky Way’s thick disk and halo therefore rely on  $J\text{--}K$  color (see Figure 2). Late-type subdwarfs<sup>1</sup> are broken down into groupings as follows: subdwarf (“sd”,  $[\text{m}/\text{H}] \approx -0.5$ ), extreme subdwarf (“esd”,  $[\text{m}/\text{H}] \approx -1.0$ ), and ultra subdwarf (“usd”,  $[\text{m}/\text{H}] \approx -1.5$ ). As can be seen in Figure 2, to reach halo-like “usd” metallicities via Roman  $J\text{--}K$  photometric selection, we need to probe down to a (Vega system)  $J\text{--}K$  color of  $\approx 0$  mag, corresponding to an AB  $J\text{--}K$  color of  $-0.9$  mag.

#### 3.1. Proposed HLWAS F213 Survey

We advocate for an augmentation to the HLWAS to include observations using the F213 filter that span the full  $\sim 2,000$  square degree HLWAS footprint and match the total science integration time for each of the other HLWAS imaging bands (F106, F129, F158, F184). As there are four other HLWAS imaging bands, our proposed F213 coverage would represent only an incremental (25%) increase in the total imaging survey time required for HLWAS. For the HLWAS science integration time in F129 (the most  $J$ -like of the WFI imaging filters), we adopt a per-exposure science integration time of 146 seconds<sup>2</sup> and a number of dithers<sup>3</sup> equal to 6 ( $146 \times 6 = 876$  seconds of total science integration). Per the Roman WFI exposure time calculator<sup>4</sup>, 876 seconds of total science integration in the F213 bandpass results in a point source limiting magnitude of 24.6 AB at  $10\sigma$ . This  $10\sigma$  F213 depth of 24.6 AB, while not deep enough to fully match the HLWAS F129 sensitivity (see Appendix A), is nevertheless dramatically deeper than that of any other existing or planned wide-area  $K$ -band survey. The next-deepest wide-area  $K$ -band survey is Vista Hemisphere Survey (VHS; McMahan et al. 2013), with a  $10\sigma$  point source depth of 19.25 mag AB, *more than 5 mags shallower*. The proposed Roman F213 depth and area at  $K$ -band will benefit not only low-mass stellar science, but also studies of dust-embedded systems (early star forming regions, embedded protostars, Wolf-Rayets) and very high-redshift sources (e.g.,  $\text{H}\alpha$  at  $z \approx 2$ , Balmer break at  $z > 4.5$ ).

#### 3.2. Combination with the Roman Grism

The wide-field Roman observations represent a Rosetta Stone for decoding the history of the Milky Way and microphysics within brown dwarfs, but to frame the matter, we consider the reference survey presented by Wang et al. (2022). Above we proposed a key addition to the HLWAS in the form of equivalent  $K$ -band imaging, but here we expressly call out the power of the notional survey’s four existing filters (F106  $Y$ , F129  $J$ , F158  $H$ , and F184  $HK$ ) and grism spectroscopy from  $1.0\text{--}1.9 \mu\text{m}$  with a uniform dispersion of  $> 10.8 \text{ \AA}/\text{pix}$ . The slitless spectroscopy will be collected over four independent position angles of  $\Delta\theta \in (5^\circ, 175^\circ, 185^\circ, 355^\circ)$  with respect to some fiducial angle that is driven by orbital or solar-avoidance considerations.

The spectra of brown dwarfs contain a wealth of information regarding the molecular inventory, physical properties (temperature, surface gravity, age), and dominant chemical processes of substellar atmospheres. The interpretation of spectra toward solving for these quantities requires both high-fidelity atmospheric models that can replicate the

<sup>1</sup> In the context of late-type stars and brown dwarfs, the term ‘subdwarf’ means a metal-poor object.

<sup>2</sup> [https://roman.gsfc.nasa.gov/high\\_latitude\\_wide\\_area\\_survey.html](https://roman.gsfc.nasa.gov/high_latitude_wide_area_survey.html)

<sup>3</sup> <https://roman.gsfc.nasa.gov/science/rsig/2021/RSIG-HLS.pdf>

<sup>4</sup> [https://roman.gsfc.nasa.gov/science/WFI\\_technical.html](https://roman.gsfc.nasa.gov/science/WFI_technical.html)

thermal flux received from these objects as well as powerful statistical inference methods to estimate the parameters that make up the model. Near- to mid-infrared brown dwarf spectra contain prominent absorption features of  $\text{H}_2\text{O}$ ,  $\text{CH}_4$ , and  $\text{NH}_3$  as well as alkali metals for the coolest objects (Lodders 2003; Kirkpatrick 2005; Cushing et al. 2011). Measuring these species can help uncover the atmospheric C/O ratio as well as the overall metal-to-hydrogen level (m/H). To this end, there have been several studies using near-infrared spectra that have coupled these facets in order to place robust constraints on key atmospheric quantities of brown dwarfs. Furthermore, planned grism spectroscopy during the HLWAS will provide an internal calibration of photometric color selection of ultracool dwarfs.

### 3.3. Connection to Other Survey Missions

Rubin/LSST (Ivezić et al. 2019) photometry will be highly valuable and complementary to HLWAS imaging for the color selection of distant, metal-poor ultracool dwarfs. At our proposed F213 sensitivity, the  $i-J$  color along Figure 2’s horizontal axis would use Rubin/LSST for  $i$ -band and Roman F129 as a stand-in for  $J$ -band. Rubin/LSST  $z$  and  $y$  bands will also be helpful for color-based ultracool dwarf selections in combination with HLWAS imaging. We assume that Rubin/LSST and HLWAS will overlap due to the importance of Rubin/LSST optical photometry for photometric redshift estimation.

It is also expected that the Euclid Wide Survey (Euclid Collaboration et al. 2022) will overlap with HLWAS. Given that there will likely be a several year gap between Euclid’s  $J$  coverage of the HLWAS footprint and Roman’s F129 HLWAS observations, it may be possible to perform kinematic selection of distant halo brown dwarfs using Euclid-Roman proper motions at  $J/\text{F129}$ . However, the Euclid wide  $10\sigma$   $J$  depth will be 23.25 AB, equating to an F213 depth of 24.15 AB for selecting halo-metallicity ultracool dwarfs. This Euclid-Roman limit is  $\approx 0.5$  mag brighter than that of our proposed F213 HLWAS survey, translating to a  $2\times$  reduction in volume and hence halo ultracool dwarf sample size. Furthermore, Gaia has illustrated that many metal poor stars do not belong to the halo, such that the F213 filter is needed for color selection of low-metallicity ultracool dwarfs in the thick disk. The combination of Roman HLWAS color selection and Euclid-Roman kinematic analysis will be very powerful for both identifying and characterizing distant ultracool dwarfs

## 4. SCIENTIFIC IMPACT

The effect of metal-poor conditions on the formation of very-low-mass objects is presently unknown, with theoretical predictions ranging from a dearth to an excess at relatively low masses (e.g., Bromm 2013; Chabrier et al. 2014). At present, the Wide-Field Infrared Survey Explorer (WISE; Wright et al. 2010) is the best resource for discovering low-metallicity substellar objects. Whereas WISE can probe  $T_{\text{eff}} \lesssim 1400$  K subdwarfs to just  $\sim 50$  pc (detecting  $\lesssim 10$  such objects; Schneider et al. 2021; Meisner et al. 2021; Brooks et al. 2022), Roman HLIS F129 in combination with our proposed Roman HLIS F213 coverage should reach  $\sim 1.7$  kpc, a  $> 1,700\times$  enhancement in volume sampled. This dramatically expanded sample of metal-poor ultracool dwarfs will permit accurate space density measurements as a function of metallicity, for the first time strongly constraining the effect of metallicity on star formation into the substellar mass regime. Roman imaging discoveries and grism characterization of distant metal-poor ultracool dwarfs will provide the first ever complete low-metallicity spectral sequence throughout the L and T type spectral classes. Roman parallaxes of metal-poor dwarfs (see Appendix B) will further provide the first ever metal-poor luminosity sequence throughout the L and T regimes. The distances probed at ultracool temperatures will far exceed Gaia, enabling studies of Galactic structure and evolution through expanded ultracool dwarf samples observed with Roman. Lastly, the HLWAS combination of Roman F129/F213 imaging plus grism spectroscopy will trace out the stellar/substellar boundary’s metallicity dependence (e.g., Burgasser et al. 2004; Zhang et al. 2017) in far greater detail than ever before.

## REFERENCES

- Aganze, C., Burgasser, A. J., Malkan, M., et al. 2022, ApJ, 924, 114, doi: [10.3847/1538-4357/ac35ea](https://doi.org/10.3847/1538-4357/ac35ea)
- Borysow, A., Jorgensen, U. G., & Zheng, C. 1997, A&A, 324, 185
- Brandt, T. D., Dupuy, T. J., Bowler, B. P., et al. 2020, AJ, 160, 196, doi: [10.3847/1538-3881/abb45e](https://doi.org/10.3847/1538-3881/abb45e)
- Bromm, V. 2013, Reports on Progress in Physics, 76, 112901, doi: [10.1088/0034-4885/76/11/112901](https://doi.org/10.1088/0034-4885/76/11/112901)
- Brooks, H., Kirkpatrick, J. D., Caselden, D., et al. 2022, AJ, 163, 47, doi: [10.3847/1538-3881/ac3a0a](https://doi.org/10.3847/1538-3881/ac3a0a)
- Burgasser, A. J., McElwain, M. W., Kirkpatrick, J. D., et al. 2004, AJ, 127, 2856, doi: [10.1086/383549](https://doi.org/10.1086/383549)

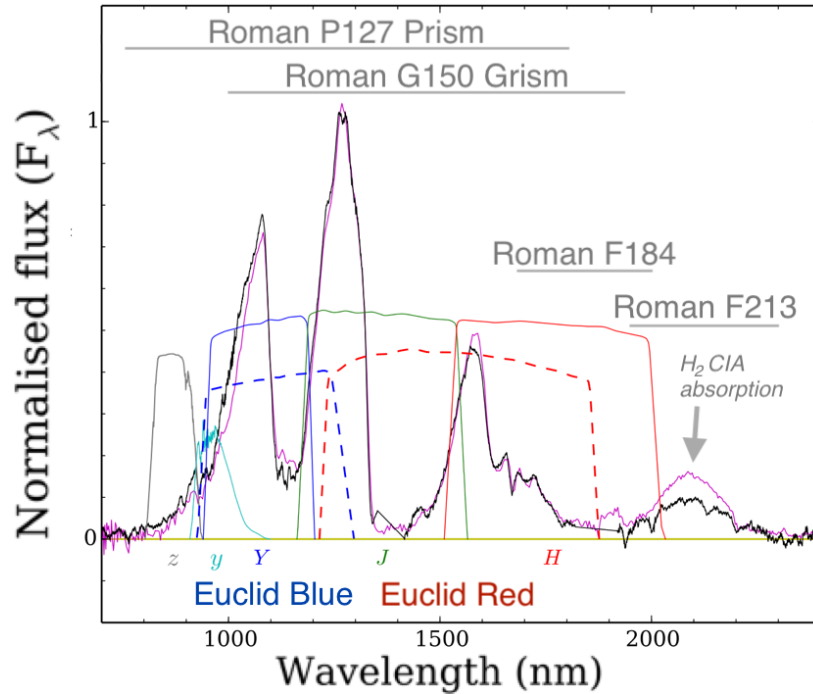


**Figure 1.** Adapted from Figure 12 of Zhang et al. (2019). The purple spectrum is that of an approximately solar metallicity T5.5 dwarf, whereas the black spectrum is that of a T5.5 subdwarf with  $[m/H] \approx -0.5$ . The dominant signature of low metallicity for such cool objects ( $T_{\text{eff}} \approx 1100$  K) in the near-infrared occurs at  $K$ -band, redward of  $2 \mu\text{m}$ , where enhanced  $\text{H}_2$  CIA absorption at low metallicity suppresses fluxes and thus leads to characteristically bluer  $J-K$  colors (bluer F129–F213 colors, in the context of Roman). Euclid’s blue and red filters are shown as dashed curves. The Rubin/LSST  $zy$  filters and Euclid’s  $YJH$  filters are also shown as solid curves. Gray horizontal lines show Roman’s prism, grism, F184, and F213 wavelength ranges. Only Roman F213 can probe the signature enhancement in  $\text{H}_2$  CIA indicative of low metallicity (gray arrow).

Burgasser, A. J., Kirkpatrick, J. D., Brown, M. E., et al. 2002, *ApJ*, 564, 421, doi: [10.1086/324033](https://doi.org/10.1086/324033)

Chabrier, G. 2003, *PASP*, 115, 763, doi: [10.1086/376392](https://doi.org/10.1086/376392)

Chabrier, G., Hennebelle, P., & Charlot, S. 2014, *ApJ*, 796, 75, doi: [10.1088/0004-637X/796/2/75](https://doi.org/10.1088/0004-637X/796/2/75)

Chung, S. J., Zhu, W., Udalski, A., et al. 2017, *ApJ*, 838, 154, doi: [10.3847/1538-4357/aa67fa](https://doi.org/10.3847/1538-4357/aa67fa)

Cushing, M. C., Kirkpatrick, J. D., Gelino, C. R., et al. 2011, *ApJ*, 743, 50, doi: [10.1088/0004-637X/743/1/50](https://doi.org/10.1088/0004-637X/743/1/50)

Euclid Collaboration, Scaramella, R., Amiaux, J., et al. 2022, *A&A*, 662, A112, doi: [10.1051/0004-6361/202141938](https://doi.org/10.1051/0004-6361/202141938)

Gagné, J., Faherty, J. K., Mamajek, E. E., et al. 2017, *ApJS*, 228, 18, doi: [10.3847/1538-4365/228/2/18](https://doi.org/10.3847/1538-4365/228/2/18)

Hallakoun, N., & Maoz, D. 2021, *MNRAS*, 507, 398, doi: [10.1093/mnras/stab2145](https://doi.org/10.1093/mnras/stab2145)

Ivezić, Ž., Kahn, S. M., Tyson, J. A., et al. 2019, *ApJ*, 873, 111, doi: [10.3847/1538-4357/ab042c](https://doi.org/10.3847/1538-4357/ab042c)

Kilic, M., Bergeron, P., Dame, K., et al. 2019, *MNRAS*, 482, 965, doi: [10.1093/mnras/sty2755](https://doi.org/10.1093/mnras/sty2755)

Kirkpatrick, J. D. 2005, *ARA&A*, 43, 195, doi: [10.1146/annurev.astro.42.053102.134017](https://doi.org/10.1146/annurev.astro.42.053102.134017)

Kirkpatrick, J. D., Martin, E. C., Smart, R. L., et al. 2019, *ApJS*, 240, 19, doi: [10.3847/1538-4365/aaf6af](https://doi.org/10.3847/1538-4365/aaf6af)

Kirkpatrick, J. D., Gelino, C. R., Faherty, J. K., et al. 2021, *ApJS*, 253, 7, doi: [10.3847/1538-4365/abd107](https://doi.org/10.3847/1538-4365/abd107)

Kroupa, P. 2001, *MNRAS*, 322, 231, doi: [10.1046/j.1365-8711.2001.04022.x](https://doi.org/10.1046/j.1365-8711.2001.04022.x)

Leggett, S. K., Tremblin, P., Phillips, M. W., et al. 2021, *ApJ*, 918, 11, doi: [10.3847/1538-4357/ac0cfe](https://doi.org/10.3847/1538-4357/ac0cfe)

Lindgren, L., Babusiaux, C., Bailer-Jones, C., et al. 2008, in *A Giant Step: from Milli- to Micro-arcsecond Astrometry*, ed. W. J. Jin, I. Platais, & M. A. C. Perryman, Vol. 248, 217–223, doi: [10.1017/S1743921308019133](https://doi.org/10.1017/S1743921308019133)

Line, M. R., Marley, M. S., Liu, M. C., et al. 2017, *ApJ*, 848, 83, doi: [10.3847/1538-4357/aa7ff0](https://doi.org/10.3847/1538-4357/aa7ff0)

Linsky, J. L. 1969, *ApJ*, 156, 989, doi: [10.1086/150030](https://doi.org/10.1086/150030)

Lodders, K. 2003, *ApJ*, 591, 1220, doi: [10.1086/375492](https://doi.org/10.1086/375492)

Lodieu, N., Hambly, N. C., & Cross, N. J. G. 2021, *MNRAS*, doi: [10.1093/mnras/stab401](https://doi.org/10.1093/mnras/stab401)

Luhman, K. L., & Hapich, C. J. 2020, *AJ*, 160, 57, doi: [10.3847/1538-3881/ab96bb](https://doi.org/10.3847/1538-3881/ab96bb)

McMahon, R. G., Banerji, M., Gonzalez, E., et al. 2013, *The Messenger*, 154, 35

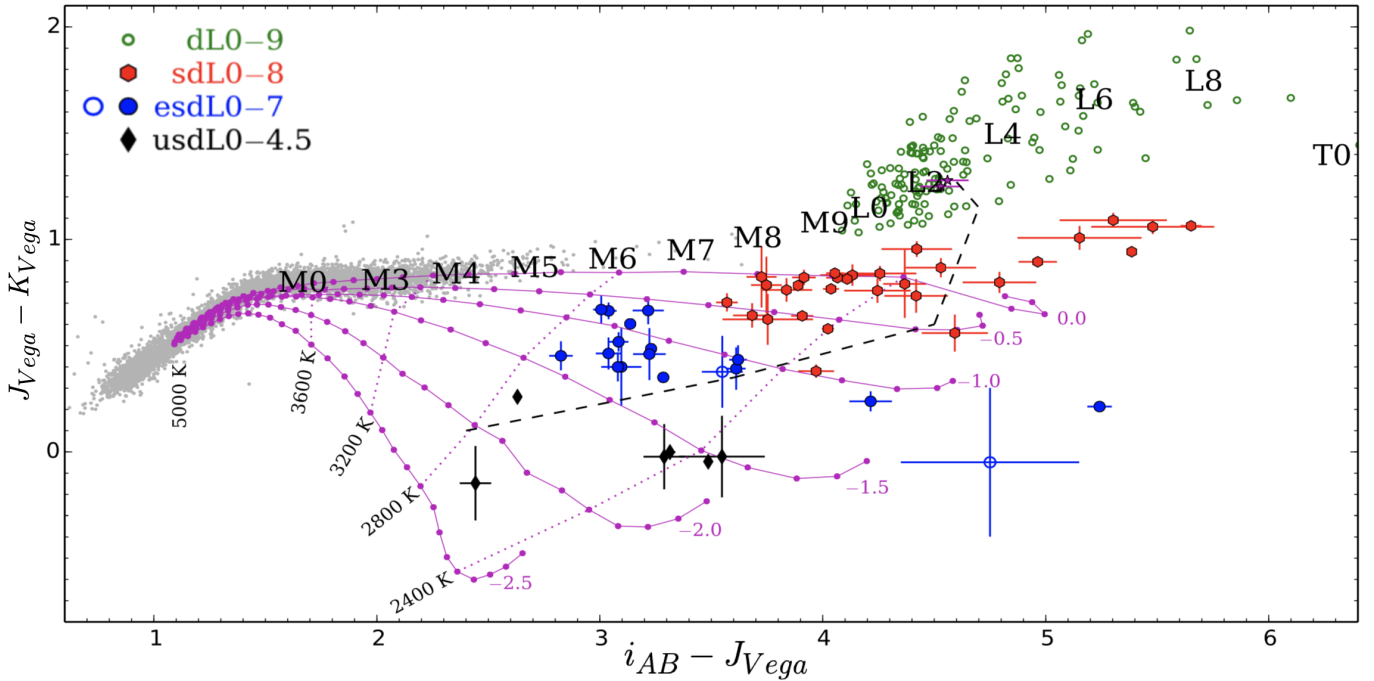


**Figure 2.** Adapted from Figure 17 of Zhang et al. (2018).  $J-K$  color (vertical axis) is critical for selecting ultracool dwarf members of the Milky Way’s thick disk and halo, due to enhanced  $H_2$  CIA absorption at low metallicity which leads to relatively blue  $J-K$  color. Note that the vertical axis is a Vega system  $J-K$  color rather than an AB system  $J-K$  color; these Vega versus AB color variants differ by a  $\approx 0.9$  mag offset, with the AB color being lower. In the context of our proposed HLWAS F213 coverage and metal-poor dwarf selection, F129 plays the role of  $J$ -band and F213 plays the role of  $K$ -band i.e., we would use F129–F213 color as a stand-in for  $J-K$ . For photometric redshift purposes, HLWAS is engineered to overlap with Rubin/LSST, so for the  $i-J$  color along the horizontal axis, it would be possible to simply cross-match Roman catalog data with Rubin/LSST catalog data to obtain  $i$ -band magnitudes. For the horizontal axis, F129 would again play the role of  $J$ -band. Further work is needed to assess the impact of contamination from non-stellar sources in this color-color diagram, though proper motions from Roman alone, Roman+Euclid, and/or Roman+Rubin should help to reliably isolate Milky Way objects. Blue open circles represent esdL objects with relatively uncertain photometry.

Meisner, A. M., Schneider, A. C., Burgasser, A. J., et al. 2021, ApJ, 915, 120, doi: [10.3847/1538-4357/ac013c](https://doi.org/10.3847/1538-4357/ac013c)

Ryan, Jr., R. E., Hathi, N. P., Cohen, S. H., & Windhorst, R. A. 2005, ApJL, 631, L159, doi: [10.1086/497368](https://doi.org/10.1086/497368)

Schneider, A. C., Meisner, A. M., Gagné, J., et al. 2021, ApJ, 921, 140, doi: [10.3847/1538-4357/ac1c75](https://doi.org/10.3847/1538-4357/ac1c75)

Theissen, C. A. 2018, ApJ, 862, 173, doi: [10.3847/1538-4357/aaccfa](https://doi.org/10.3847/1538-4357/aaccfa)

Wang, Y., Zhai, Z., Alavi, A., et al. 2022, ApJ, 928, 1, doi: [10.3847/1538-4357/ac4973](https://doi.org/10.3847/1538-4357/ac4973)

Wright, E. L., Eisenhardt, P. R. M., Mainzer, A. K., et al. 2010, AJ, 140, 1868, doi: [10.1088/0004-6256/140/6/1868](https://doi.org/10.1088/0004-6256/140/6/1868)

Zhang, Z. H., Burgasser, A. J., Gálvez-Ortiz, M. C., et al. 2019, MNRAS, 486, 1260, doi: [10.1093/mnras/stz777](https://doi.org/10.1093/mnras/stz777)

Zhang, Z. H., Homeier, D., Pinfield, D. J., et al. 2017, MNRAS, 468, 261, doi: [10.1093/mnras/stx350](https://doi.org/10.1093/mnras/stx350)

Zhang, Z. H., Galvez-Ortiz, M. C., Pinfield, D. J., et al. 2018, MNRAS, 480, 5447, doi: [10.1093/mnras/sty2054](https://doi.org/10.1093/mnras/sty2054)

## APPENDIX

## A. AN HLWAS DEPTH-MATCHED F213 SURVEY?

To fully leverage the exceptional F129 depth of Roman’s HLWAS coverage, for which we adopt a value of 26.9 AB ( $5\sigma$  point source), we would need to accurately measure a  $J-K$  (F129–F213) AB color of  $\approx -0.9$  mag at the F129 faint end. For the F129 faint end, we adopt the  $10\sigma$  depth of 26.15 mag AB, as we do not wish to have per-band magnitude errors larger than 0.1 mag entering into the F129–F213 color determination. To match this  $10\sigma$  F129 depth of 26.15 mag AB in F213 at the lowest metallicities for ultracool dwarfs, we would need to achieve a  $10\sigma$  F213 depth of  $26.15 + 0.9 = 27.05$  mag AB. Per the Roman WFI exposure time calculator, this would require a total science integration time of  $\approx 74,000$  seconds, dramatically longer than the HLWAS per-band total science integration time for F106 through F184 ( $\lesssim 1,000$  s). Therefore, we deem this “depth-matched” F213 HLWAS option far less practicable than the F213 survey proposed in §3.1, and consider only the latter in terms of scientific impact for metal-poor ultracool dwarf science. For all exposure time calculations in this work, we adopt the faintest selectable zodiacal light option, as we expect the HLWAS footprint will avoid the ecliptic plane to maximize sensitivity.

## B. ASTROMETRIC CONSIDERATIONS

Although the cadence of the HLWAS is likely not sufficient to measure accurate parallaxes, there are some considerations that could be taken into account when HLWAS is combined with data from, for example, the Roman High-Latitude Time Domain Survey (HLTDS) which will observe at a higher cadence. Roman observations acquired close to maximum parallax factor would majorly benefit any parallax measurements using Roman and hence catalyze additional ultracool dwarf science. Indeed, such a strategy was adopted by WISE, enabling parallaxes for faint red sources beyond the reach of Gaia (Theissen 2018). To maximize the precision of Roman parallax plus proper motion astrometric solutions, it would be beneficial to: 1) use the maximum time baseline possible, obtaining the first epoch of observations early in the mission, and the last close to the end of the nominal mission, which will allow precise proper motions to be measured; and 2) obtain observations close to maximum and minimum parallax factors to enable eventual parallax measurements from the combined survey data.